



# Optics Letters

## Single-shot quantitative phase microscopy based on color-multiplexed Fourier ptychography

JIASONG SUN,<sup>1,2,3</sup> QIAN CHEN,<sup>1,2,\*</sup> JIALIN ZHANG,<sup>1,2,3</sup> YAO FAN,<sup>1,2,3</sup> AND CHAO ZUO<sup>1,2,3,4</sup>

<sup>1</sup>School of Electronic and Optical Engineering, Nanjing University of Science and Technology, No. 200 Xiaolingwei Street, Nanjing, Jiangsu 210094, China

<sup>2</sup>Jiangsu Key Laboratory of Spectral Imaging & Intelligent Sense, Nanjing, Jiangsu 210094, China

<sup>3</sup>Smart Computational Imaging Laboratory (SCILab), Nanjing University of Science and Technology, Nanjing, Jiangsu 210094, China

<sup>4</sup>e-mail: zuochao@njjust.edu.cn

\*Corresponding author: chenqian@njjust.edu.cn

Received 30 April 2018; revised 5 June 2018; accepted 18 June 2018; posted 18 June 2018 (Doc. ID 330676); published 11 July 2018

We present a single-shot quantitative phase imaging (QPI) method based on color-multiplexed Fourier ptychographic microscopy (FPM). Three light-emitting diode (LED) elements with respective R/G/B channels in a programmable LED array illuminate the specimen simultaneously, providing triangle oblique illuminations matching the numerical aperture of the objective precisely. A color image sensor records the light transmitted through the specimen, and three monochromatic intensity images at each color channel are then separated and utilized to recover the phase of the specimen. After one-step deconvolution based on the phase contrast transfer function, the obtained initial phase map is further refined by the FPM-based iterative recovery algorithm to overcome pixel-aliasing and improve the phase recovery accuracy. The high-speed, high-throughput QPI capabilities of the proposed approach are demonstrated by imaging HeLa cells mitosis *in vitro*, achieving a half-pitch resolution of 388 nm across a wide field of view of 1.33 mm<sup>2</sup> at camera-limited frame rates (50 fps). © 2018 Optical Society of America

**OCIS codes:** (110.1758) Computational imaging; (100.5070) Phase retrieval; (110.0180) Microscopy; (100.3010) Image reconstruction techniques.

<https://doi.org/10.1364/OL.43.003365>

Quantitative phase imaging (QPI) is one of the rapidly evolving microscopy techniques for recovering the phase distribution of transparent biological and technical specimens [1]. It enables label-free and stain-free optical imaging of biological samples *in vitro* and allows unbiased quantitative biological studies, such as the measurement of cell volume, membrane fluctuations, cell mass, and growth dynamics. Over the past decades, many QPI methods have been developed, including digital holography [2], low-coherence interferometry [3], transport of intensity equation [4], differential phase contrast (DPC) [5], and Fourier ptychographic microscopy (FPM) [6]. Among this wide array of existing QPI methods, FPM is perhaps

the most promising approach to realizing high-resolution, high-throughput imaging without requiring any mechanical scanning, which is of crucial importance for high-content quantitative analysis of multiple events in large cell colonies over extended periods of time.

Sharing its roots with synthetic aperture imaging and ptychographic phase retrieval, FPM overcomes the space-bandwidth product (SBP) limit of a conventional microscope by synthesizing a wide-field, high-resolution complex image from multiple angle-variably illuminated, low-resolution images. However, in order to fulfill the inherent data redundancy requirement in conventional FPM, a large number of raw images are often collected, precluding imaging at high temporal resolution. A lot of methods have been proposed to improve the data acquisition efficiency of FPM, either computationally [7–10] or physically [11]. Multiplexing and coherent state decomposition strategies allow us to turn on multiple light-emitting diodes (LEDs) simultaneously, accelerating the image acquisition process and shortening the exposure time [8,9]. By combining DPC with random multiplexing, Tian *et al.* proposed a source-coded FPM technique which reduces the number of acquired images to 21 [10]. Though large-SBP imaging of live cells *in vitro* at 1.25 Hz was demonstrated, the speed is still inadequate for many high-speed QPI applications. Recently, a single-shot FPM setup based on diffractive beam splitting has been introduced [11], inspired by the beam splitting scheme applied in conventional ptychography [12]. However, since multiple low-resolution images are arranged on a single image sensor with a limited sensor area, the imaging field of view (FOV) has to be compromised significantly, compared with conventional FPM.

To improve the data collection efficiency without sacrificing the SBP, in this Letter, we present a single-shot FPM method based on color-multiplexed illuminations for achieving QPI of live cells. This approach starts from an initial phase estimate obtained by a one-step deconvolution in the Fourier domain based on the weak phase transfer function (PTF) of FPM. Considering a pure phase object [Fig. 1(A1)] with complex transmission function  $t(\mathbf{x}) = e^{i\phi(\mathbf{x})} \approx 1 + i\phi(\mathbf{x})$ , the intensity spectrum [Fig. 1(B2)] for a bright-field image under oblique illumination [Fig. 1(B1)] in FPM can be represented as [13]

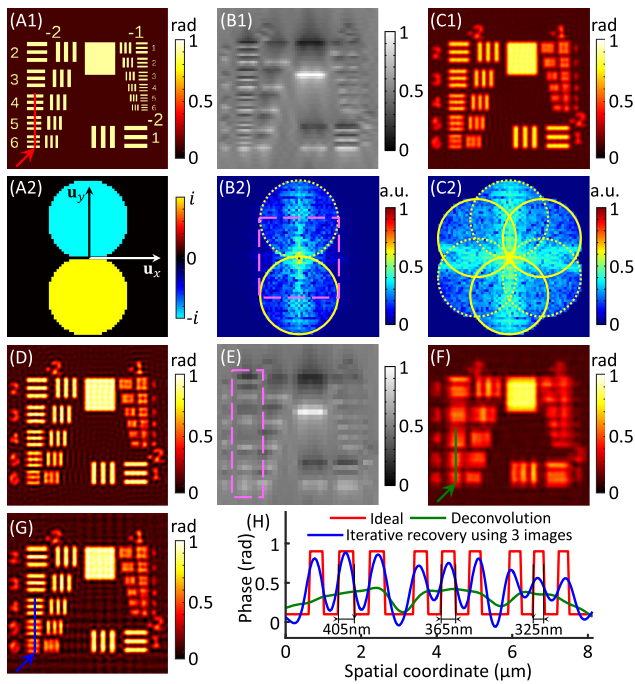


**Fig. 1.** (A1) Simulated ideal pure phase object. (A2), (B1), (B2) PTF, intensity map, and frequency spectrum of a bright-field image under oblique illumination in FPM when  $NA_{\text{ill}} = NA_{\text{obj}}$  and the imaging pixel size matches  $2NA_{\text{obj}}$ . (C1), (C2) Recovered initial phase map and its frequency spectrum after single-step deconvolution. (D) Phase map obtained from FPM-based iterative algorithm. (E)–(G) Intensity image, initial phase map recovered from interpolation and deconvolution, and final iteratively reconstructed phase image when the imaging pixel size is defined by  $NA_{\text{obj}}$ . (H) Line profiles illustrating phase retrieval accuracy of deconvolution and FPM-based algorithms when the pixel size matches  $NA_{\text{obj}}$ .

$$I_j(\mathbf{u}) \approx \delta(\mathbf{u}) + i\Phi(\mathbf{u})[P(\mathbf{u} + \mathbf{u}_j) - P(\mathbf{u} - \mathbf{u}_j)], \quad (1)$$

where  $\mathbf{u}_j$  represents the corresponding frequency shift vector induced by the tilted illumination, and  $P(\mathbf{u})$  presents the pupil function of the objective (an ideal low-pass filter with the cutoff frequency of  $\frac{NA_{\text{obj}}}{\lambda}$ ). Here we adopt a weak object approximation and neglect the high-order convolution terms of  $\Phi(\mathbf{u})$  to linearize the phase retrieval problem. In Eq. (1), the delta function is associated with the uniform background intensity, and the second term denotes the contribution of the object phase. Thus, the PTF of FPM for bright-field imaging is simply denoted as

$$\text{PTF}_j(\mathbf{u}) = i[P(\mathbf{u} + \mathbf{u}_j) - P(\mathbf{u} - \mathbf{u}_j)]. \quad (2)$$

Equation (2) reveals a very important fact that only under-matched tilted illuminations ( $NA_{\text{ill}} = NA_{\text{obj}}$ ), the two anti-symmetrical (positive and negative) components of the PTF, will not cancel each other out near the origin [see Fig. 1(A2)], making the low-frequency phase components contribute to image formation. In other words, in order to retrieve the low-frequency phase component correctly, we should guarantee that the LED is precisely located at the edge of objective numerical aperture (NA). The example shown in Fig. 1(B2) verifies that the intensity spectrum corresponding to one matched illumination angle has almost the same frequency support as the PTF [Fig. 1(A2)], covering two central symmetric apertures in the

Fourier domain. Therefore, only three LEDs are sufficient to cover the support area of six frequency apertures with hexagonal configurations, as shown in Fig. 1(C2). Here we simulated three LEDs illuminated in a 525 nm wavelength with  $0.4NA_{\text{ill}}$  matching the  $NA_{\text{obj}}$ , while the imaging pixel size (325 nm) is selected to match the Nyquist frequency of  $2NA_{\text{obj}}$  (328 nm, half-pitch). Similar to the DPC method [14], we can adopt a single-step deconvolution to obtain an initial estimate of the phase distribution [Fig. 1(C1)] according to Eq. (3):

$$\Phi(\mathbf{u}) = \frac{\sum_{j=1}^N [I_j(\mathbf{u}) - \delta(\mathbf{u})] \text{PTF}_j^*(\mathbf{u})}{\sum_{j=1}^N |\text{PTF}_j(\mathbf{u})|^2}, \quad (3)$$

where  $*$  denotes the complex conjugate.

As illustrated in Fig. 1(C1), through the theoretical resolution, a limit of  $2NA_{\text{obj}}$  can be achieved by the deconvolution, the recovered phase value is underestimated by about 10%. This is because the weak object approximation is not strictly satisfied in our example (phase value varies between  $[0.1, 0.9]$  rad), leading to reconstruction errors. As observed in Fig. 1(B2), there still remains some weak frequency components [which may result from the nonlinear terms of  $\Phi(\mathbf{u})$ ] falling outside the theoretical support, which are not considered in the deconvolution model. Therefore, to compensate for the phase discrepancy, the initial phase map is taken as the input of the FPM-based iterative recovery algorithm. As the three intensity images corresponding to three LEDs can only provide the intensity constraint for three aperture regions, we introduce an extra uniform intensity constraint, which can be regarded as a regularizer for the full complex wavefront in the object space at the end of each iteration and, after that, the frequency content of three opposite aperture regions can be updated automatically. As shown in Fig. 1(D), accurate phase value can be recovered after the FPM iteration, which is valid beyond the limit of weak phase. In addition, the FPM-based phase refining algorithm can also be used to overcome the pixel-aliasing problem in phase deconvolution because the imposed spatial sampling limit of FPM is only the Nyquist frequency defined by  $NA_{\text{obj}}$  [15], instead of  $2NA_{\text{obj}}$ . Figure 1(E) shows the insufficiently sampled intensity image when the camera pixel size (650 nm) just fulfills the Nyquist frequency defined by  $NA_{\text{obj}}$ . Under this condition, the high-frequency components of the PTF will alias into the central part of the spectrum [the purple dashed square region in Fig. 1(B2)], which corresponds to the maximum frequency support determined by the pixel size of the camera. Note that interpolating the image before deconvolution cannot remove the aliasing, resulting in significant degradation of image resolution [Fig. 1(F)]. However, by further invoking the FPM-based iterative refinement, the theoretical resolution limit corresponding to  $2NA_{\text{obj}}$  can be recovered again, as shown in Fig. 1(G). The resolution improvement can be more clearly observed by examining corresponding line profiles, as shown in Fig. 1(H). These results demonstrate the twin advantages of FPM-based refinement over conventional DPC-based schemes: higher accuracy and anti-aliasing. It should also be noted that although the conventional FPM further allows us to recover the pupil function, along with the sample function, such an aberration compensation feature can no longer be fulfilled in our approach due to the insufficient data redundancy provided by the limited number of raw images.

Based on the above analysis, we know that three images are sufficient to achieve high-efficiency QPI with resolution up to

$2NA_{\text{obj}}$ . However, it still requires sequential acquisition of three intensity images with different illumination angles. To further improve the imaging speed, the three images can be combined into one color image based on color-coded illuminations, similar to color-multiplexed DPC methods [16,17]. Inspired by this idea, we developed a color-multiplexed FPM approach for QPI in a single shot. Our method, termed single-shot FPM (SFPM), is based on a standard FPM setup reformed from a commercial inverted microscope (IX73, Olympus) [Fig. 2(A)], but employs three LEDs with respective R/G/B channels in the programmable LED array (4 mm spacing, central wavelength 632/525/465 nm) to generate color-coded triangle oblique illuminations matching a  $10\times$ ,  $0.4NA$  objective (UPlanSApo  $10\times$ , Olympus) precisely [see Fig. 2(B1)]. A sample image [Fig. 2(C1)] is recorded by a color image sensor (PCO.edge 3.1,  $2048 \times 1536$  resolution,  $6.5 \mu\text{m}$  pixel pitch, 50 Hz) and is then separated into three monochromatic intensity images corresponding to each LED based on a color-leakage correction algorithm [18]. Since the original imaging pixel size ( $650 \text{ nm}$ ) is insufficient for the Nyquist frequency of  $2NA_{\text{obj}}$  required in the deconvolution model, image interpolation is required before deconvolution to generate an initial phase map. Then an FPM-based iterative recovery algorithm is applied to overcome pixel-aliasing and improve the phase recovery accuracy [Fig. 2(D1)]. The whole algorithm flowchart of SFPM is summarized in Fig. 2(E). In this case, from each color image, we can reconstruct the phase distribution of a dynamic pure phase object every  $0.02 \text{ s}$  interval, corresponding to a single-shot QPI frame rate of  $50 \text{ Hz}$ .

It should be noted that, different from the previous case where the three LEDs have the same wavelength, the tri-color illumination results in uneven coverage of Fourier space. [See the Fourier spectrum at the top right corner in Fig. 2(D1).] In order to achieve near-isotropic imaging resolution, we provide an alternating SFPM illumination scheme. Different from Fig. 2(B1), the three RGB LEDs rotate in a circle constituting illumination pattern 2 [Fig. 2(B2)], and these two patterns illuminate the sample alternately (switch every  $0.02 \text{ s}$ ). For stationary or slowly varying samples, the two color images acquired at the moments of  $t(n)$  and  $t(n-1)$  can be used in SFPM reconstruction to cover 12 apertures in Fourier domain, achieving higher recovery accuracy while reducing the QPI frame rate by half ( $25 \text{ Hz}$ ).

To evaluate the QPI accuracy and resolution improvement of SFPM, we experimentally measured a real pure phase

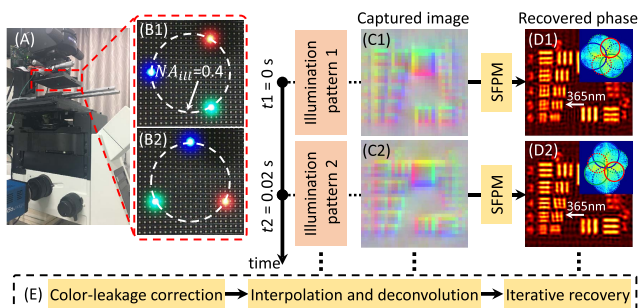


**Fig. 2.** Color-multiplexed illumination patterns and the flowchart of SFPM technique. (A) SFPM system. (B1), (B2) Color-multiplexed illumination patterns. (C1)–(C2) Captured color images at  $t_1 - t_2$ . (D1)–(D2) Recovered phase maps corresponding to each color image. (E) Flowchart of SFPM.

resolution target [quantitative phase microscopy target (QPT), Benchmark Technologies Corporation, U.S.]. Figure 3(A1) shows a bright-field full-FOV image of the sample, which is captured under incoherent white-light illumination. Since the sample is a pure phase object, this bright-field image has very little intensity contrast, satisfying the uniform intensity constraint applied in SFPM. The boxed region in Fig. 3(A1) is enlarged, as presented in Fig. 3(A2), showing an original half-pitch resolution of  $615 \text{ nm}$  (Group 9, Element 5), which agrees well with the original imaging pixel size. Afterwards, we implemented our SFPM technique to recover the phase distribution of the target and derive sub-pixel resolution. Figure 3(B) presents an enlarged view of one color-multiplexed raw image corresponding to illumination pattern 1; Figs. 3(C1) and 3(C2) display the recovered phase maps using an SFPM algorithm without and with iterative refinement. To evaluate the phase retrieval accuracy quantitatively, line profiles across the square target of Group 8, Element 2 are extracted and compared in Fig. 3(D1). After converting the recovered phase value to the physical thickness (the refractive index of QPT material is about 1.52), we found that the recovered result using SFPM with iterative refinement (red dashed line) matches well with the nominal height value ( $200 \text{ nm}$ ) (purple dashed line) with a root-mean-square error of  $8.3 \text{ nm}$ . However, the height value recovered without iterative refinement is again underestimated (green dashed line). To further distinguish the highest achievable resolution, the line profiles of resolution target Group 10, Elements 2–4 along the  $y$ -axis (corresponding to half-pitch resolution of  $435$ ,  $388$ , and  $345 \text{ nm}$ , respectively) are extracted and shown in Fig. 3(D2). The significant improvement of resolution delivered by the iterative refinement [from  $615$  ( $\text{green line}$ ) to  $388 \text{ nm}$  ( $\text{red line}$ )] can be clearly observed. These results have demonstrated that SFPM can achieve a half-pitch

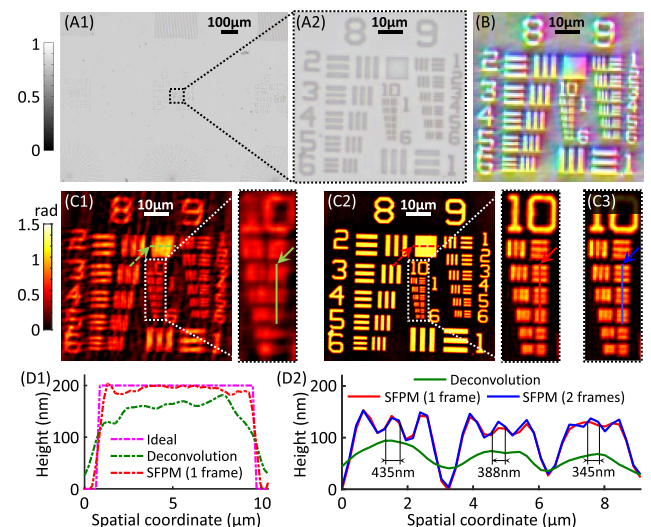


**Fig. 3.** Experimental QPI of a pure phase resolution target. (A1) Bright-field full-FOV image of the target under incoherent white-light illumination. (A2) Enlarged view of the black boxed region in (A1). (B) Captured color image when illumination pattern 1 is lit up. (C1), (C2) Recovered phase maps using SFPM without and with iterative refinement. (C3) Recovered phase map with two illumination patterns. (D1), (D2) Line profiles of the recovered pure phase specimen in (C1)–(C3).

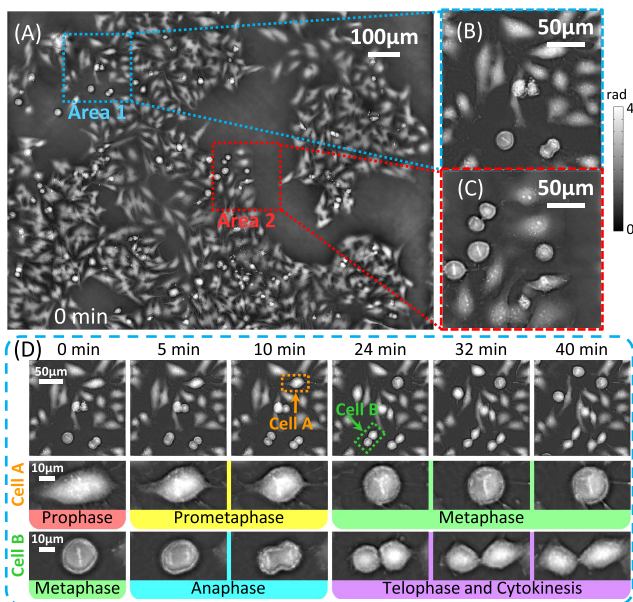


**Fig. 4.** Single-shot QPI of HeLa cells *in vitro* using SFPM with an acquisition time of 0.02 s per frame. (A) One frame of the full-FOV phase reconstruction. (B), (C) Enlarged images of the blue-boxed and red-boxed regions in (A). (D) Sample frames of a reconstructed video (see Visualization 1) for a zoom-in view of blue-boxed regions in (A) at 5–8 min intervals across 40 min.

resolution of 388 nm across a wide FOV of 1.33 mm<sup>2</sup> at camera-limited frame rates (50 fps), corresponding to a space–bandwidth–time product of 441 megapixels/s [nearly approaching the theoretical limit of the camera’s data transfer rate (472 megapixels/s, 9.44 megapixels captured in 0.02 s)]. It should be noted that if the two-frame recovery scheme is utilized for such a static sample, the reconstruction quality, as well as the image resolution (especially along the *y* direction) can be further improved slightly, as shown in Figs. 3(C3) and 3(D2) [from 388 (red line) to 345 nm (blue line)].

At last, we implemented SFPM to observe unstained HeLa cells *in vitro* across 40 min with a video acquisition speed of 50 Hz. Since the cells are unstained in this experiment, they can be regarded as pure phase objects approximately. An example frame from a reconstructed large-SBP phase video (see Visualization 1) is shown in Fig. 4(A). Two selected zoom-in regions are shown in Figs. 4(B) and 4(C), and several frames of the video for the blue-boxed Area 1 at different moments are shown in the top row of Fig. 4(D). In Figs. 4(B) and 4(C), subcellular features, such as cytoplasmic vesicles and pseudopodium, are clearly visualized. In addition, plasmid migration and other organelle motions can be clearly observed in the QPI video. As shown in the bottom two rows of Fig. 4(D), two arrow-pointed cells (cells A and B) are enlarged to present different typical mitosis phases and the morphological evolution of cells during the mitotic cycle across 40 min. Since each high resolution phase image was recovered within only 0.02 s, all these retracting, extending, reorganizing, migrating, and maturing processes were recovered accurately without motion blur,

which can be extremely valuable to researchers, biomedical specialists, and biologists who are interested in cytomorphology, cytokinetics, and cytogenetics.

In conclusion, we have proposed a single-shot FPM technique based on color-multiplexed illuminations, named SFPM, to accomplish high-resolution large-SBP phase retrieval for unstained live samples *in vitro*. The investigation of the PTF for FPM reveals that when the oblique illuminations match the  $NA_{obj}$  precisely, only three monochromatic intensity images are sufficient to achieve high-accuracy phase retrieval by combining phase deconvolution and FPM iterative refinement. Based on this fact, a color-multiplexed illumination from three LEDs in R/G/B channels can efficiently provide considerable frequency support area with sufficient data redundancy, and then high-quality large-SBP QPI can be realized for pure phase industrial optical specimens and unstained biological samples in a single shot. The theoretical analysis and experimental results suggest that the SFPM is a powerful QPI technique for various high-throughput microscopic applications, such as drug discovery, cellular phenotypes characterization, and identification of disease mechanisms.

**Funding.** National Natural Science Foundation of China (NSFC) (61722506, 61505081, 11574152); Final Assembly “13th Five-Year Planquot” Advanced Research Project of China (30102070102); National Defense Science and Technology Foundation of China (0106173); Outstanding Youth Foundation of Jiangsu Province of China (BK20170034); Key Research and Development Program of Jiangsu Province, China (BE2017162); “333 Engineering” Research Project of Jiangsu Province, China (BRA2016407); Fundamental Research Funds for the Central Universities (30917011204, 30916011322).

## REFERENCES

- M. Mir, B. Bhaduri, R. Wang, R. Zhu, and G. Popescu, *Prog. Opt.* **57**, 133 (2012).
- E. Cucho, F. Bevilacqua, and C. Depeursinge, *Opt. Lett.* **24**, 291 (1999).
- H. Iwai, C. Fang-Yen, G. Popescu, A. Wax, K. Badizadegan, R. R. Dasari, and M. S. Feld, *Opt. Lett.* **29**, 2399 (2004).
- A. Barty, K. Nugent, D. Paganin, and A. Roberts, *Opt. Lett.* **23**, 817 (1998).
- S. B. Mehta and C. J. Sheppard, *Opt. Lett.* **34**, 1924 (2009).
- G. Zheng, R. Horstmeyer, and C. Yang, *Nat. Photonics* **7**, 739 (2013).
- L. Bian, J. Suo, G. Situ, G. Zheng, F. Chen, and Q. Dai, *Opt. Lett.* **39**, 6648 (2014).
- S. Dong, R. Shiradkar, P. Nanda, and G. Zheng, *Biomed. Opt. Express* **5**, 1757 (2014).
- L. Tian, X. Li, K. Ramchandran, and L. Waller, *Biomed. Opt. Express* **5**, 2376 (2014).
- L. Tian, Z. Liu, L.-H. Yeh, M. Chen, J. Zhong, and L. Waller, *Optica* **2**, 904 (2015).
- X. He, C. Liu, and J. Zhu, *Opt. Lett.* **43**, 214 (2018).
- P. Sidorenko and O. Cohen, *Optica* **3**, 9 (2016).
- J. Sun, C. Zuo, J. Zhang, Y. Fan, and Q. Chen, *Sci. Rep.* **8**, 7669 (2018).
- L. Tian and L. Waller, *Opt. Express* **23**, 11394 (2015).
- J. Sun, Q. Chen, Y. Zhang, and C. Zuo, *Opt. Express* **24**, 15765 (2016).
- Z. F. Phillips, M. Chen, and L. Waller, *PLoS ONE* **12**, e0171228 (2017).
- W. Lee, D. Jung, S. Ryu, and C. Joo, *Opt. Express* **25**, 8398 (2017).
- Y. Wu, Y. Zhang, W. Luo, and A. Ozcan, *Sci. Rep.* **6**, 28601 (2016).